Material transfer and contact optimization in MoS$_2$ nanotube devices

Robin T. K. Schock[*,1], **Stefan Obloh**[1], **Jonathan Neuwald**[1], **Matthias Kronseder**[1], **Wolfgang Möckel**[1], **Matjaž Malok**[2], **Luka Pirker**[2,3], **Maja Remškar**[2], **Andreas K. Hüttel**[1]

[1] Institute for Experimental and Applied Physics, University of Regensburg, 93053 Regensburg, Germany
[2] Solid State Physics Department, Institute Jožef Stefan, 1000 Ljubljana, Slovenia
[3] J. Heyrovský Institute of Physical Chemistry, v.v.i., Czech Academy of Sciences, 18223 Prague, Czech Republic

[*] Corresponding author: e-mail andreas.huettel@ur.de

While the promise of clean and defect-free MoS$_2$ nanotubes as quantum electronic devices is obvious, ranging from strong spin-orbit interaction to intrinsic superconductivity, device fabrication still poses considerable challenges. Deterministic transfer of transition metal dichalcogenide nanomaterials and transparent contacts to the nanomaterials are nowadays highly active topics of research, both with fundamental research and applications in mind. Contamination from transport agents as well as surface adsorbates and surface charges play a critical role for device performance. Many techniques have been proposed to address these topics for transition metal dichalcogenides in general. Here, we analyse their usage for the transfer based fabrication of MoS$_2$ nanotube devices. Further, we compare different contact materials in order to avoid the formation of a Schottky barrier.

1 Introduction Since the first experimental isolation of graphene [1], the field of two-dimensional materials has grown immensely [2–6]. One prominent group of such materials is given by transition metal dichalcogenides (TMDCs) [2], consisting of a layer of hexagonally arranged transition metal atoms (e.g., tungsten, molybdenum) sandwiched between two hexagonal layers of chalcogenides (e.g., sulfur, selenium, tellurium). MoS$_2$, a member of this group, is a typically n-doped semiconductor with a strong spin-orbit interaction. In its monolayer form, broken inversion symmetry causes spin split bands [2]. In addition, even in the monolayer limit it can be driven into intrinsic superconductivity via ionic doping [7,8]; for hole conduction, theory predicts it to be a topological superconductor [9–11].

Many attempts have been made to define quantum dots (QDs) in planar TMDC materials [12]. However, the typically large effective electron mass in the conduction band requires minuscule devices sizes at the limits of traditional lithography, and most observations so far are limited to classical, metallic Coulomb blockade [13–17] and QDs at defects [18–20]. Only very recently quantization effects have been observed in lithographically defined systems [21,22]. TMDC-based nanotubes [23] could naturally provide strong confinement in an additional dimension as well as perfect electronic boundary conditions compared to lithographically defined nanoribbons.

The challenging fabrication of long and defect free MoS$_2$ nanotubes [24], higher radii compared to CNTs [25], and the fact that only multiwall nanotubes have been isolated up to now, have so far limited research. Additionally, the TMDCs where stable and defect-free nanotubes have been produced, are typically semiconductors. Metal contacts form Schottky barriers, resulting in large contact resistances [26]. Strong Fermi level pinning has been observed [27,28], further complicating the situation. For planar TMDCs, recently remarkable advances in circumventing these barriers were made [29–31]. Regarding nanotubes, for a long time research was limited to optical and mechanical properties [32,33], and work adressing superconductivity in WS$_2$ [34]. First attempts of low temperature transport spectroscopy used metals with a suitable low work function [35,36], but these metals were shown to react with and destroy the crystal lattice of MoS$_2$ [36–38]. Only recently, using the semimetal bismuth led to a breakthrough [39].
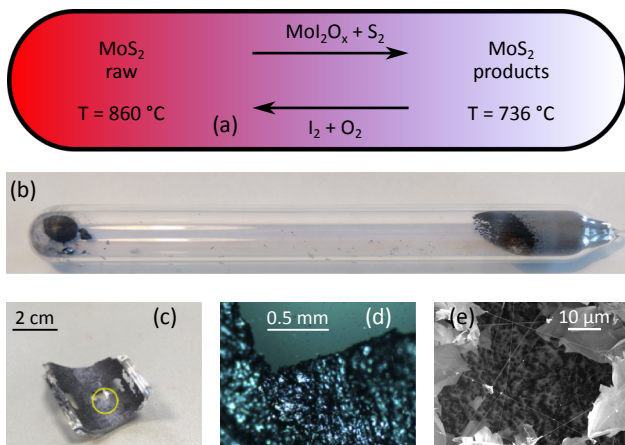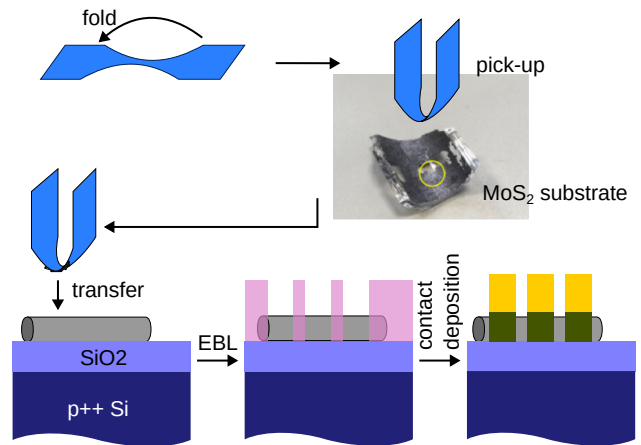
Figure 1 MoS$_2$ nanotube growth: a) schematic of the chemical transport growth reaction, b) photograph of a growth ampoule containing the source material and the reaction result, c), d), optical images of the resulting material on a piece of a broken ampoule, e) scanning electron micrograph of the material displaying MoS$_2$ nanotubes and flakes.

Figure 2 Schematic of the "Scotch tape" (or "Nitto tape") method as applied here. First a piece of Nitto Denko ELP BT-150E-CM tape is cut into a strip narrowing in the middle. Then the strip is folded and softly pressed onto the MoS$_2$ nanotube growth substrate, a piece of the original quartz ampoule. This way nanotubes are picked up and can then be placed onto a receiving p-doped Si-SiO$_2$ substrate. Subsequently, using a standard electron beam lithography (EBL) process, metal evaporation / sputtering, and lift off, contacts are defined on the nanotubes.

Here, we utilize state of the art transfer techniques adapted from 2D materials [40, 41] and classical semiconductor fabrication to build electronic devices integrating MoS$_2$ nanotubes. We compare these techniques in terms of device yield and describe their effects on the device. Overall, surprisingly, the devices fabricated with the classical "Scotch tape" method perform better then any of the more sophisticated transfer techniques. Additionally, we investigate several contact materials, extending our previously published results [39]. Still bismuth remains so far the best candidate for contacting MoS$_2$ nanotubes.

2 MoS$_2$ nanotube growth In this work we use MoS$_2$ nanotubes grown by an iodine-assisted chemical transfer process [24, 42, 43]. This technique utilizes the migration of the gas phase of a metal compound along a temperature gradient from an area of vaporisation to an area of crystallisation. A halogen, in this case iodine, functions as transport agent.

The precursor, bulk crystalline MoS$_2$, is given into a quartz glass ampoule together with iodine I$_2$, see Fig. 1(a,b). The ampoule is subsequently evacuated and sealed by locally melting the quartz glass. It is then heated up in a tube oven under presence of a temperature gradient, with the precursor MoS$_2$ placed at the hotter end. Remaining oxygen O$_2$ emitted from the quartz glass ampoule walls also participates in the reaction. The precursor reacts according to MoS$_2$ + I$_2$ + O$_2$ $\longrightarrow$ MoI$_2$O$_x$ + S$_2$, with the gaseous products then migrating along the temperature gradient to the cooler recrystallisation area, see Fig. 1(a) [42]. There, the reverse process, MoI$_2$O$_x$ + S$_2$ $\longrightarrow$ MoS$_2$ + I$_2$ + O$_2$, takes place. Subsequently the transport agents diffuse back to the hotter end, leading to a

continuous process as long as the temperature gradient is maintained and feed material is present.

Over a growth period of approximately $500\,$h, clean and long nanotubes with a very low defect density, form on the growth side, accompanied by ribbon-like collapsed nanotubes, platelets, flakes, and more complex structures. After a slow cool-down, the quartz glass ampoule is broken apart in order to access the grown and deposited material. Example images of growth results can be found in Fig. 1(c,d,e).

3 Transfer and assembly techniques Over the past decade, for research on 2d materials many different material transfer and assembly techniques have been developed, and this process is still onging. In the following we discuss the usage of some of these methods for MoS$_2$ nanotube devices. In general, more complex transfer methods are developed to avoid contamination by the transfer agents and achieve cleaner results. As an example, the anthracene crystal based method detailed below in Section 3.5 has been used by Otsuka *et al.* with carbon nanotubes, leading to photoluminescence spectra fully comparable to as-grown macromolecules and thus indicating negligible contamination effects [40].

3.1 The "Scotch tape" method A very straightforward procedure to integrate MoS$_2$ nanotubes into electronic devices is the classical "Scotch tape", "blue tape", or "Nitto tape" method initially developed for graphene [1], as illustrated in Fig. 2. Nitto Denko ELP BT-150E-CM adhesive tape is pressed onto the raw MoS$_2$ material on a piece of the glass ampoule. Then the same piece

of tape is pressed onto a Silicon wafer with a thermally grown $500\,\mathrm{nm}$ thick oxide layer and predefined chromium-gold position markers. This randomly transfers nanotubes, flakes, and other MoS_2 nanostructures onto the chip surface at an adjustable surface density.

In order to contact specific nanotubes, their position on the chip is then determined by optical microscopy. Surprisingly, even small diameter MoS_2 nanotubes can be detected this way; we attribute the clear visibility to their outstanding optical properties [38,44]. The optical images, including position markers, are used as base for the design of contact geometries. The chip is then spin-coated with polymethyl metacrylate (PMMA) resist; after a standard electron beam lithography process, the contact metallization is deposited onto the exposed parts of the nanotubes and lift-off in hot acetone is performed, see Fig. 2 and the discussion of the different materials below.

3.2 Suspending nanotubes between contacts

This process can be altered in order to reduce the disorder caused by the amorphous SiO_2 surface and its surface charges; from carbon nanotubes it is well-known that suspending the nanostructures leads to significantly better spectroscopic results [45,46]. Prior to stamping the nanotubes onto sample, a PMMA resist is deposited onto the surface. The stamp transfer works equally well for the blank SiO_2 surface and the hardened PMMA layer. After the transfer, a second PMMA layer is then spincoated onto the first resist, such that the nanotubes are ideally located at the interface between both layers. After EBL, the nanotubes are suspended first between the two resist layers and, after the contact metal deposition, by the contacts themselves.

For the two resist layers, either a 50k PMMA bottom layer, $1\,\%$ to $4\,\%$ weight dissolved in anisol, was used resulting in a resist thickness range of $20\,\mathrm{nm}$ to $60\,\mathrm{nm}$ comparable to or less than the nanotube diameters, or for a higher likelyhood of a finite gap between chip substrate and nanotube a $9\,\%$ PMMA 200k layer leading to a resist thickness of about $200\,\mathrm{nm}$. For the top layer in either case $9\,\%$ PMMA 200k was applied. Different metallizations were tested, see also the discussion and the SEM images in Fig. 8, Section 4.3 below, where the quality of the resulting contacts is discussed. A typical thin contact layer would consist of $40\,\mathrm{nm}$ bismuth and $50\,\mathrm{nm}$ gold, both thermally evaporated; later experiments tested thicker but similar metallization layers.

3.3 Polydimethylsiloxane (PDMS) transfer

Polydimethylsiloxane (PDMS) is a silicon based polymer widely used in 2D material science as a substrate and as a transfer agent [41,47]. This is due to its flexibility and viscoelastic properties, which make the transfer of 2D flakes (and nanotubes) between different substrates possible.

Here, PDMS was primarily used to transfer quasi-two dimensional hexagonal Boron nitride (hBN) and few layer graphite onto SiO_2 substrates with predefined gold-structures on them, as highly conductive back gate and
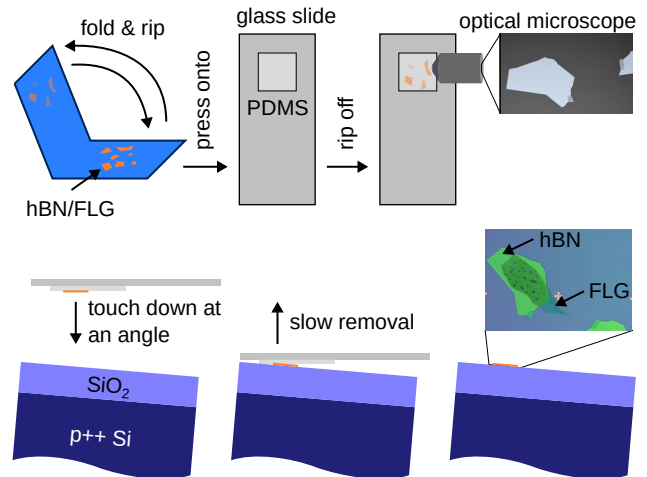

Figure 3 Schematics of the polydimethylsiloxane (PDMS) transfer method, mostly used for few layer graphite (FLG) and hexagonal Boron nitrite (hBN) flake transfer. First a piece of Nitto tape is cut into a strip and pressed upon the bulk substrate of the transfer material, e.g., hBN. Then the strip is folded onto itself and ripped apart repeatedly in order to thin down the material. By pressing a piece of PDMS of $\sim 1\,\mathrm{cm} \times 1\,\mathrm{cm}$ onto the Nitto tape and ripping it off, some of the flakes are transferred onto the PDMS. After determining the position of a flake with an optical microscope, the flakes are transferred onto a SiO_2/Si substrate.

crystalline gate isolator without dangling bonds. Literature on bilayer graphene has amply demonstrated that this sort of material stack reduces disorder from the amorphous surface of SiO_2 as well as provides a very homogeneous electric field [48–52]. While the transfer does not directly involve the MoS_2 nanotubes, we include it here for completeness.

Material transfer is achieved by at first pressing a ribbon of Nitto tape onto a bulk piece of the material in question, thereby retrieving a small amount of the 2D material, see Fig. 3. Subsequently, the tape is folded, pressed together, and then ripped apart in order to break up the bulk stacks into smaller stacks and potentially monolayers of the 2D materials. This process is repeated at least 10 times.

A piece of a flat PDMS film, commercially available as Gelpak Gelfilm, is attached to a glass slide and pressed onto the adhesive tape with the exfoliated 2D materials. Using a very fast peel-off, some of the flakes are transferred onto the PDMS film. The film is then inspected in an optical microscope. Finally, flakes of the desired size and thickness are carefully pressed onto a receiving SiO_2 substrate and then remain on the surface when peeling off the PDMS very slowly.

3.4 Polycarbonate (PC) transfer

This method builds upon the two previous recipes, with an additional component for avoiding contaminations. First a thin layer of polycarbonate (PC), or more precisely poly(bisphenol A carbonate), is fabricated through coating a glass slide with
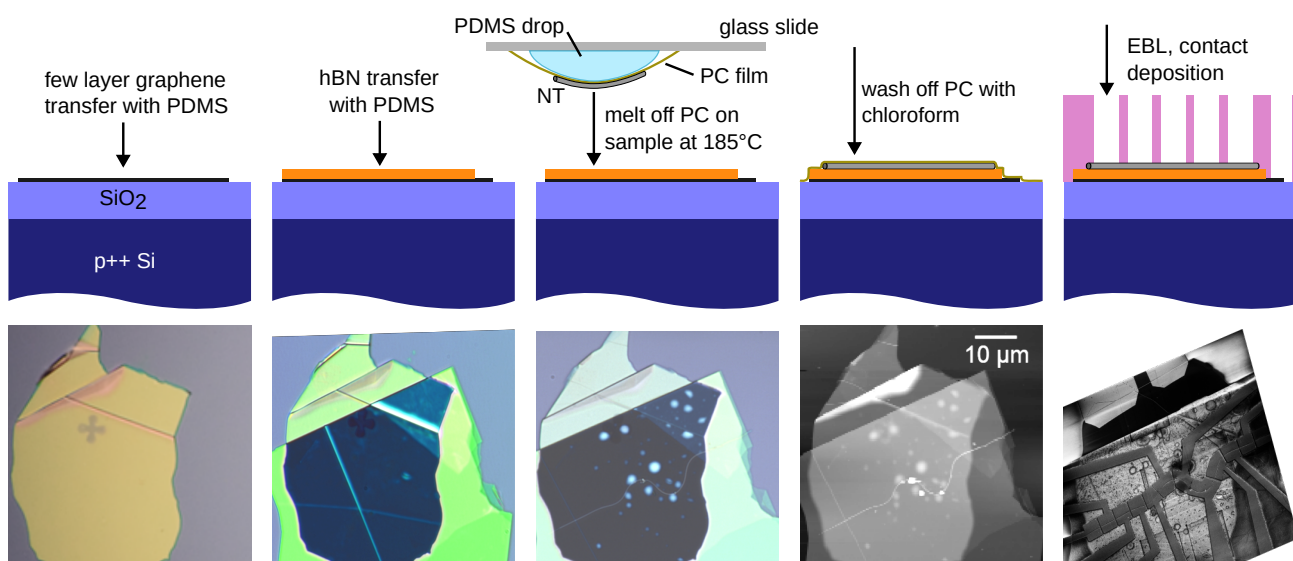
Figure 4 Schematics of the polycarbonate (PC) assisted transfer method. In the first step, few layer graphene (FLG) and hBN are transferred with the "PDMS method" (see Fig. 3) and stacked upon each other. Then a previously prepared strip of a thin PC film is placed and fixed upon a PDMS droplet on a glass slide. In an xyz-stage, a nanotube is picked up from a silicon wafer (prepared with the "Scotch tape method", see Fig. 2). The nanotube is placed upon the FLG-hBN heterostack, and the PC is molten at $185\,^\circ\mathrm{C}$. Afterwards, the PC is washed off with chloroform and the nanotube is contacted through standard EBL processing.

a chloroform-PC solution of $4\,\%$. The coating is subsequently air-dried. The resulting PC layer is slowly peeled off the glass slide using an adhesive tape with a cutout area in the middle. The PC-tape stack is then placed onto a pre-made PDMS droplet on another glassslide, where it is secured such that the exposed PC layer is stretched over the droplet. The resulting PC-film coated droplet is then carefully pressed onto a substrate with an isolated, previously exfoliated nanotube or flake, heated to 130°C, and slowly peeled off, effectively picking up the material.

The resulting stack, consisting of the flake or nanotube, the PC layer, and the PDMS droplet on a glass carrier, is subsequently pressed onto a receiving substrate and heated to 185°C, causing the PC to melt, see Fig. 4. As the PDMS is lifted, the liquefied PC with the attached nanomaterial structure remains on the sample. Finally, the PC layer is gently washed off in hot chloroform for 15 minutes, leaving the nanotube or flake on the substrate.

Compared to direct transfer with only PDMS, this procedure has two main advantages. Due to the melting of the PC film, it is possible to transfer materials which adhere stronger to PDMS than to the receiving substrate. Further, as there is no direct contact between the flakes/nanotubes and the PDMS, any contamination from PDMS is washed off together with the PC in the chloroform rinsing step.

3.5 Anthracene assisted transfer In case the PC film transfer introduces to too much contamination, a recently developed replacement procedure utilizes anthracene crystals as alternative intermediate transfer agent between PDMS and the flakes or nanotubes [40]. To implement this method, also illustrated in Fig. 5, we first

grew anthracene crystals on glass slides suspended $1\,\mathrm{mm}$ above granular anthracene heated to $80\,^\circ\mathrm{C}$ in an ambient atmosphere. In order to grow large and thin single crystals with a size of about $1\,\mathrm{mm}^2$, following Otsuka *et al.* [40] a commercial permanent marker was used to draw black lines on the glass slide, see Fig. 5. In the marked, dark regions, the growth of crystals is suppressed; crystals growing nearby can extend above this region and then reach larger sizes. The initial publication used a permanent marker of type KOKUYO PM-41B; we found the type STAEDLER permanent Lumocolor S, Nr. 313-9 to be a suitable replacement. After a growth period of about $12\,\mathrm{h}$, large and homogeneous anthracene single crystals form on the slides.

With an optical microscope in a transfer setup, suitable crystals were chosen and picked up with a PDMS droplet, see Fig. 5. Similar to the PC based method, the anthracene crystal was pressed upon a flake or nanotube and the substrate was subsequently heated to a temperature of above $80\,^\circ\mathrm{C}$ in order to increase the adhesion of the anthracene to the object to be transferred. Then, the nanotube, anthracene, and PDMS stack was rapidly peeled off (in under a second) to ensure that the anthracene adheres more strongly to the PDMS than to the SiO_2 chip surface. In order to deposit the nanomaterial at the top of the stack, it was pressed upon the desired location of the receiving chip, heated to a temperature above $90\,^\circ\mathrm{C}$, and very slowly peeled off over a duration of about one minute, which left the anthracene with the transferred stack on the surface of the chip. The anthracene crystal was then sublimated by
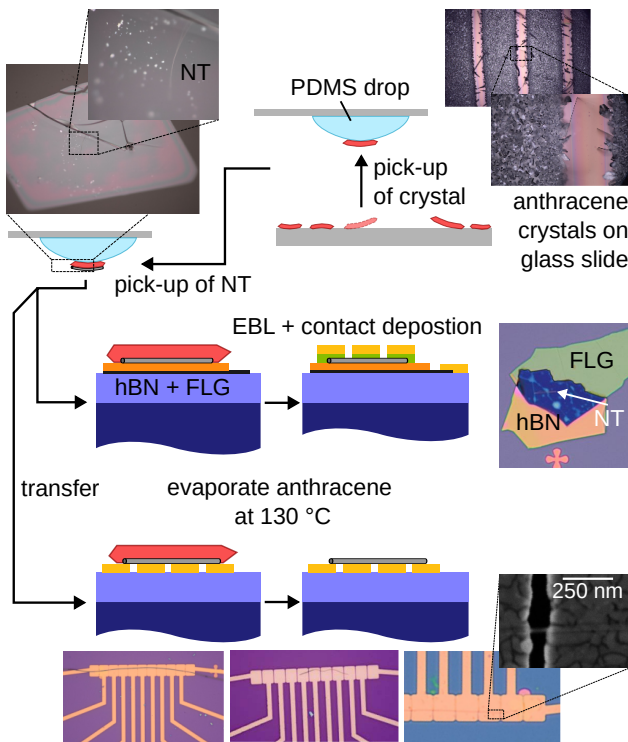
Figure 5 Anthracene crystal assisted transfer of a nanotube. First, anthracene crystals are grown on a glass slide. Then, a large anthracene crystal is picked up with a PDMS drop. With this, a nanotube, exfoliated with the scotch tape method, or a 2D flake (hBN or FLG) can be picked up. These can then be either placed onto a heterostack (middle part) or transferred onto predefined contacts (lower part). The anthracene crystal with the material is pressed onto the chip and remains there if peeled off slowly. After that, the anthracene is sublimated by heating the device above $130\,°C$.

heating to a temperature above $130\,°C$; it typically leaves no visible contamination residues.

As shown in Fig. 5, this method allows for two different approaches to device fabrication. Either a heterostack can be assembled with subsequent deposition of top contacts, or the nanotube can be placed upon predefined contacts with trenches between them. As the anthracene evaporates in an ambient atmosphere, without the need of any wet chemical processing, there is no danger of ripping off thin layers or nanotubes due to surface tension [40]. Using predefined contacts is obviously limited to contact materials which do not form an insulating oxide barrier in ambient atmosphere, unless additional encapsulation steps are performed.

4 Contact engineering For all the deposition of nanotubes and/or layer assembly of devices, achieving good electrical contacts to the nanomaterial is of central importance. In particular, here we talk about transparent and non-destructive contacts [39]: transparent meaning having a low resistance and Ohmic behaviour, and non-destructive

meaning that the contact fabrication does not significantly damage the molecular and thereby electronic structure of the nanomaterial.

For planar, quasi-twodimensional MoS_2, a large amount research has been invested into this topic worldwide, with the primary objective of Ohmic contacts for MoS_2-based field effect transistors. As with many other TMDC materials, strong Schottky barriers typically form at the semiconductor-metal interface [26,53]. The precise mechanisms involved in their formation have long been under discussion. While the mismatch of the metal work function certainly contributes, see the discussion below, additionally strong Fermi level pinning takes place at the interface [54,27,55,28].

In the case of MoS_2 nanotubes, the reduced geometry poses additional difficulties. An edge contact to a MoS_2 flake is effectively a one-dimensional interface; the same edge contact to a nanotube however zero-dimensional. Further, while graphene has been shown to make good contacts to planar MoS_2 and other TMDC [56], so far no such success has been achieved by depositing a "flat" graphene or graphite layer onto a "round" nanotube or vice versa — an observation which can likely be attributed to the shape mismatch.

4.1 Impact of the contact material Several different approaches to avoid the formation of a Schottky barrier at metallic contacts to MoS_2 have been proposed so far. Primarily these revolve around the selection of the contact material. In classical semiconductor technology, a Schottky barrier is minimized by adapting the metal work function to the semiconductor. For MoS_2 with an electron affinity of $\lambda_{MoS_2} = 4.0\,eV$, this means selecting a *low-work function metal* such as titanium or scandium [31, 36,37]. In the following we name this a *type-I contact*. As demonstrated in [36], scandium can be used to contact MoS_2 nanotubes, however, serial charge traps make Coulomb blockade spectroscopy difficult. In hindsight, the origin of these charge traps is obvious – the chemically reactive metal destroys the MoS_2 layer structure already during deposition [37].

Inserting a thin insulating layer (e.g., an insulating hBN monolayer) as a *transparent tunneling barrier* which at the same time prevents Schottky barrier formation has been attempted with some success on 2d materials [57–60]. Accordingly this was also tested for MoS_2 nanotubes, see the discussion below, and named *type-II contact*. Local doping in the contact areas is another technique transferred from existing semiconductor technology [61,62]. For nanotubes, the small relevant surface area makes this difficult to implement; in addition, surface dopants immediately lead to potential irregularities that would pose problems in low temperature measurements. Since copper doping has shown promise in other works [63], we also have tested bulk copper contacts.

Recently, it was discovered, that the use of *semimetals* was a promising way to avoid the formation of strong
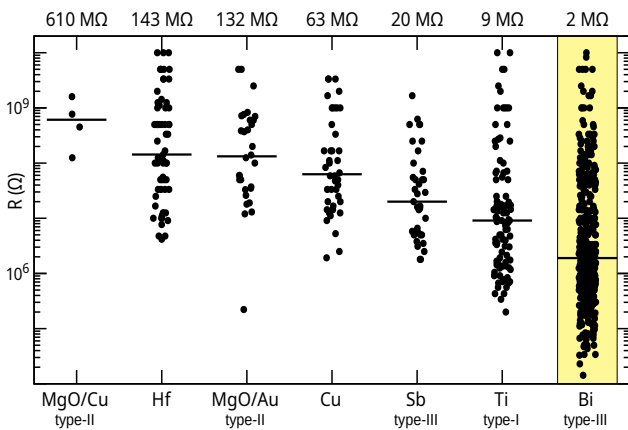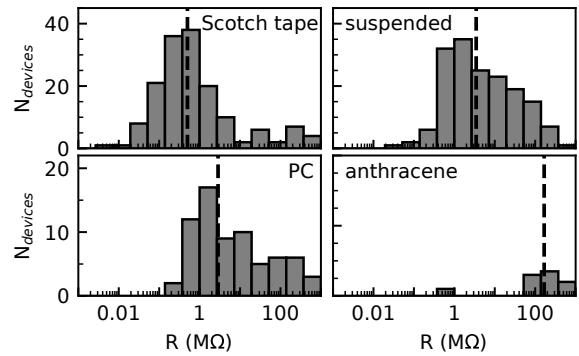
Figure 6 Two terminal resistances of MoS_2 nanotubes and nanoribbons contacted with different contact materials. Each point in the graph corresponds to the room temperature resistance measured between two contacts on a nanotube or nanoribbon. Additionally, the median resistance for each material is marked with a black line. Clearly, bismuth leads to the smallest median resistance, an order of magnitude smaller than the second best tested material titanium. Part of the data has already been shown in [39].

Figure 7 Two terminal resistance distributions of bismuth-contacted nanotube devices, for four different material transfer methods – "Scotch tape" deposition (Section 3.1), suspended nanomaterial (Section 3.2), polycarbonate-assisted deposition (Section 3.4), and anthracene-assisted deposition (Section 3.5).

Schottky barriers at a MoS_2 interface [29]. In the interface region of a semiconductor and a metal, hybridization of the electronic bands of the semiconductor and the metal leads to so-called metal-induced-gap-states (MIGS) and via them to Fermi level pinning [64]. The density of states (DOS) of a semimetal however approaches zero at the Fermi level, leading to a corresponding reduction in MIGS. This in turn reduces stability of the Schottky barrier and makes Ohmic contacts possible [29,30,39]. Graphene has already been used to contact planar MoS_2 [56], attempts with MoS_2 nanotubes have failed so far however, most likely due to the mismatch in shape / geometry. This leads us to the elements bismuth [29,39] and antimony [30, 65], already highly successful for planar materials, as contact layers. This approach is in the following named *type-III contact*.

The devices prepared in this work were measured under ambient conditions. The two-point resistance was determined by applying a constant bias voltage of $10\,mV$ and measuring the resulting current. The resulting values for different contact materials are shown as scatter plots in Fig. 6, with the median of each material given as horizontal line and written out above the corresponding column. Bismuth-based semi-metal contacts (i.e., *type-III*) clearly outperformed all other tested materials, with a median two-point resistance value of $R_{Bi} = 2\,M\Omega$ [29,39]. This confirms corresponding work on planar MoS_2 as well as our own previous publication [39].

The material with the second best median two-point resistance was titanium. It is a metal with a well suited work function for n-type conduction band contacts to MoS_2 (i.e., *type-I*), however has also shown to be highly reactive [37].

Similar results and disadvantages have been seen for scandium [36]. As such, even though the room temperature results are promising, charge traps and potential irregularities at the contacts will likely make low-temperature transport spectroscopy challenging.

Aside bismuth, also the semimetal antimony has been used to successfully make contacts to planar TMDC materials [30]. However, for our nanotubes the results using antimony were already significantly worse, with a median value $R_{Sb} = 20\,M\Omega$. Note that Li *et al.* only achieved their best contact resistances with antimony grown in the $(01\bar{1}2)$ direction, depositing the contacts under elevated temperatures of about $100\,°C$ [30]. In contrast, here, the antimony was deposited at room temperature, and no clear statement on its crystal orientation was possible. In addition, compared to planar MoS_2, where a topmost layer can be matched by the crystal structure of the contact material, nanotubes expose a curved surface to the semimetal. This likely prevents even locally the formation of a single crystalline layer with a matching structure.

Further material combinations tested include gold and copper – as well-conducting metals with a large electronic density of states – on top of a thin MgO tunnel barrier, i.e., *type-II* contacts. As visible in Fig. 6, in both cases the resulting two-point resistances are comparatively high. Even given the scatter and the still relatively small number of data points, further investigations seem not worthwhile, with median two-point resistance values of $610\,M\Omega$ and $132\,M\Omega$.

4.2 Impact of the transfer technique In Fig. 7, we compare the observed two terminal resistances of devices prepared with different transfer techniques. In all cases, bismuth has been used as the contact layer. As clearly visible from the figure, so far, the simplest "Scotch tape" transfer technique shows the best results, with a much larger number of devices exhibiting two terminal resistances below $1\,M\Omega$. Both suspending the nanomaterial (see Sec. 3.2) and PC transfer (see Sec. 3.4) seem to have a negative im-

pact on the fraction of devices produced with a two-point resistance below $1\,M\Omega$. Additionally, much more devices with resistances above $10\,M\Omega$ can be observed, indicating a reduced quality of the contacts.

The validity of the evaluation is limited insofar as the fabrication using more complex methods took mostly place at a later time and used later nanomaterial growth batches; a hypothetical change in clean room chemicals quality, raw material properties (which we do not have any further indications of), etc., would materialize similarly in the plots.

As for the anthracene method, only a very small number of devices was tested so far. All the data in Fig. 7 for anthracene devices stems from contacts to a total number of 4 nanotubes prepared in two different ways; it can only tentatively indicate that this approach also reduces contact quality. The chips with device resistances above $100\,M\Omega$ were prepared with contacts predefined by EBL procedure and a channel length of about $100\,nm$. In the two devices on one nanotube with resistances below $1\,M\Omega$, the nanotube was transferred onto gold contacts pre-sliced with the beam of a focused ion beam (FIB) system. The channel length in these devices was at about $50\,nm$ much smaller than that of other device types, which may contribute to slightly lower device resistance. Further, it is conceivable that the Ga^+ ions deposited by the FIB beam in the vicinity of the trenches dope the surface of the nanotubes and therefore lower the Schottky barrier. With only one nanotube tested so far, these ideas are however only speculative and require further investigation.

4.3 SEM failure analysis The large scatter of the resistance data points in Fig. 6 and Fig. 7 even in the case of nominally identical device preparation indicates that the fabrication process still has fundamental limitations. To identify problems, several devices were imaged in detail in a scanning electron microscope; example results can be seen in Fig. 8.

A possible cause of the reduced contact quality is the occurrence of gaps between the contact material on top of the tube and the surrounding material. While not occurring for carbon nanotubes due to their much smaller radius, this is a known (and sometimes intended) phenomenon when contacting elevated structures such as semiconductor nanowires. Due to the directional material deposition via thermal evaporation, a 'cap' forms on the top of the nanotube. As the cap grows, it begins to shadow a larger area below the tube, reducing growth in that region. A precise adjustment of the metal film thickness to the nanomaterial is in our case challenging since typically nanotubes and ribbons of varying size are deposited on the same chip.

Initial resistance testing of devices with different layer thicknesses suggested an optimum of electronic behaviour around the parameters of Fig. 8(a) [39]. However, if the metal films are not thick enough, the cap of contact metal on top of the nanostructure and the surrounding contact material may not consistently reach each other. This is possible in the region indicated with an arrow in the SEM im-
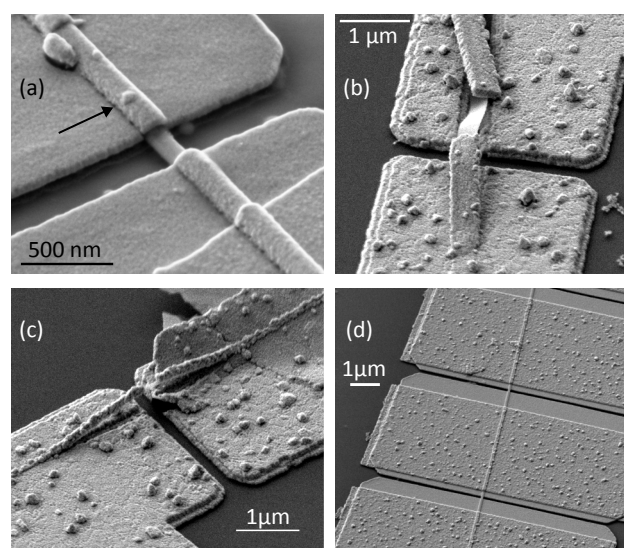
Figure 8 SEM images of devices after fabrication and probe station characterization. (a) Nanotube contacted with a bismuth layer of $40\,nm$ and a gold layer of $50\,nm$; (b) nanoribbon and (c) nanotube on the same sample contacted with a bismuth layer of $50\,nm$ and a gold layer of $100\,nm$ both evaporated under two different angles, resulting in a step-like perimeter; (d) nanotube transferred with anthracene onto $100\,nm$ gold contacts with a $\approx 100\,nm$ gaps and subsequently contacted with $25\,nm$ bismuth and $30\,nm$ gold, both evaporated at two different angles.

age of Fig. 8(a), indicating the need for a more robust contact metallization.

In addition, SEM images of devices suggest grain-based growth of the films, especially for bismuth, with corresponding fluctuation of the layer thicknesses and potential gap sizes. Even in presence of a gap, contact could still occur occasionally. This process is not limited to the suspended nanotube case, but is very likely to be more dominant there. This could further explain the wide scatter of contact resistances for all materials and the slightly worse results for devices intended to be suspended.

In order to prevent the gap formation, the contacts deposited in Fig. 8(b) were significantly thicker; in addition, thermal evaporation of the contact materials was done at two separate angles of device orientation to improve coverage. Preliminary results indicate that this could at least partially improve the contact quality; one of two devices fabricated so far had several contacts with resistances below $1\,M\Omega$. The second one, with the nanoribbon depicted in Fig. 8(b), performed much worse, clearly since almost all nanoribbons and -tubes were ripped out of the embedding material. The reason for this is unclear so far.

5 Discussion of the resistance scatter Of all tested contact materials, the bismuth-gold combination so far remains the most promising one – in combination with the least sophisticated fabrication method. Never-

theless, the observed two-point resistances scatter widely. What is the cause?

A *wide distribution of nanomaterial properties* cannot be fully excluded. The MoS_2 growth process delivers flakes, nanotubes, nanoribbons as well as breathing and twisted variants [24,66]. During the transfer process, long, straight, and thin structures are preferably selected in the optical microscope. Distinguishing nanotubes from nanoribbons and determining the precise dimensions would however require time-consuming SEM or AFM imaging, which may also lead to additional contamination or damage.

Contamination during lithography, as, e.g., organic resist residues or reactions with photoresists or -developers, is another relevant topic. Moving the fabrication away from optical lithography to electron beam lithography with its organic chemistry only has so far not led to clear improvements. Imperfect dissolution of resist layers during development is possible. While the resist remainders can in principle be removed with a brief oxygen plasma based descum process, the plasma treatment will strongly attack the sulphur surface and have an impact on its own [67–69].

PDMS or PC contamination during stamping can reduce the device quality. It is already known that PDMS contaminates the surface of 2D materials after the stamping process [40,70,71]. As both FLG and hBN were transferred using PDMS this can introduce disorder in the heterostack, degrading the quality of the backgate. Additionally, contamination on the hBN surface is in direct contact with the nanotubes and could influence its electronic properties. Finally, during the PC transfer of the nanotube, residues of PDMS may spread onto the contact suface of the nanotube. Together with contamination from the PC itself [70], these would be directly at the nanotube semimetal interface.

Insufficient metallization or metallization gaps at the contacts can, as discussed already above, particularly affect large-diameter nanomaterials and suspended structures. One may also speculate that too thick bismuth regions become non-conductive at low temperature, leading to additional resistive barriers. Metal deposition under varying angles and thicker gold cap layers should be used to mitigate these effects.

Tear-off of the nanomaterial has been observed, e.g., in Fig. 8(b,c), as also discussed above; while the nanotube or nanoribbon remains whole, it entirely or in part lifts out of the contact electrodes, taking part of the material with it. Again thicker metallization, here combined with a more careful lift-off procedure, may be required. Surface tension during drying would pull a possibly suspended nanomaterial towards the substrate; we expect this to lead to different types of damage. Nevertheless, also the use of a critical point dryer may be considered for future devices.

6 Conclusions and outlook MoS_2 nanotubes and nanoribbons have significant potential for quantum elec-

tronic devices. Here, we compare different contact materials and material transfer techniques and their effect on the contacts to these MoS_2 nanomaterials.

Regarding the contact materials, we can so far conclude that the best choice for MoS_2 nanotubes and nanoribbons is bismuth [29,39], a semi-metal leading to the minimzation of metal-induced gap states and Fermi level pinning. While for planar MoS_2 antimony, also a semi-metal, has led to record conductivities [30,65], this could not be confirmed for nanotubes. The comparison of different transfer techniques indicates that the classical "Scotch tape" method [1] in its simplicity still gives the most reliable results. We tentatively conclude that more complex fabrication procedures still pose more danger of surface contamination. A large scatter of measured resistance values remains, which can be due to several different causes. Insufficient coverage of the non-planar nanomaterial and the formation of minuscule "nano-gaps" between the contact material covering the nanotubes and the material surrounding it, even at the apparent optimal layer thickness, seems to play an important role, with surface contaminations secondary in effect.

In order to reduce the impact of the nano-gaps, multiple-angle evaporation as well as an overall thicker layer of contact material was used. First data indicate an improved likelihood of good contacts. Evaporation onto a heated device substrate as well as annealing are further approaches to be followed in the future. Regarding the reduction of potential surface contamination, O_2 and Ar plasma treatments shall be tested as next steps [67–69], as well as H_2S exposure of the devices at elevated temperature [72]. Even though clearly not all approaches apply to nanotubes and nanowires, the highly active world-wide research on planar MoS_2 field effect transistors provides a multitude of avenues to follow.

References

[1] K. S. Novoselov, A. K. Geim, S. V. Morozov, D. Jiang, Y. Zhang, S. V. Dubonos, I. V. Grigorieva, and A. A. Firsov, Science **306**(5696), 666–669 (2004).

[2] O. V. Yazyev and A. Kis, Materials Today **18**(1), 20–30 (2015).

[3] K. S. Novoselov, A. Mishchenko, A. Carvalho, and A. H. Castro Neto, Science **353**(6298), aac9439 (2016).

[4] C. Tan, X. Cao, X. J. Wu, Q. He, J. Yang, X. Zhang, J. Chen, W. Zhao, S. Han, G. H. Nam, M. Sindoro, and H. Zhang, Chemical Reviews **117**(9), 6225–6331 (2017).

[5] S. Kang, D. Lee, J. Kim, A. Capasso, H. S. Kang, J. W. Park, C. H. Lee, and G. H. Lee, 2D Materials **7**(2), 022003 (2020).

[6] S. Joseph, J. Mohan, S. Lakshmy, S. Thomas, B. Chakraborty, S. Thomas, and N. Kalarikkal, Materials Chemistry and Physics **297**, 127332 (2023).

[7] J. M. Lu, O. Zheliuk, I. Leermakers, N. F. Q. Yuan, U. Zeitler, K. T. Law, and J. T. Ye, Science **350**(6266), 1353–1357 (2015).

[8] D. Costanzo, S. Jo, H. Berger, and A. F. Morpurgo, Nature Nanotechnology **11**(4), 339–344 (2016).

[9] Y. T. Hsu, A. Vaezi, M. H. Fischer, and E. A. Kim, Nat. Commun. **8**(1), 14985 (2017).

[10] R. Oiwa, Y. Yanagi, and H. Kusunose, Phys. Rev. B **98**(6), 064509 (2018).

[11] J. Wang, X. Zhang, R. Ma, G. Yang, E. V. Castro, and T. Ma, Physical Review B **106**(13), 134513 (2022).

[12] F. M. Jing, Z. Z. Zhang, G. Q. Qin, G. Luo, G. Cao, H. O. Li, X. X. Song, and G. P. Guo, Advanced Quantum Technologies **5**(6), 2100162 (2022).

[13] Y. Li and N. Mason, From Coulomb Blockade to Resonant Transmission in a MoS2 Nanoribbon, 2013, arXiv:1312.3939.

[14] C. S. Lau, J. Y. Chee, L. Cao, Z. E. Ooi, S. W. Tong, M. Bosman, F. Bussolotti, T. Deng, G. Wu, S. W. Yang, T. Wang, S. L. Teo, C. P. Y. Wong, J. W. Chai, L. Chen, Z. M. Zhang, K. W. Ang, Y. S. Ang, and K. E. J. Goh, Advanced Materials **34**(25), 2103907 (2022).

[15] X. X. Song, D. Liu, V. Mosallanejad, J. You, T. Y. Han, D. T. Chen, H. O. Li, G. Cao, M. Xiao, G. C. Guo, and G. P. Guo, Nanoscale **7**(40), 16867–16873 (2015).

[16] X. X. Song, Z. Z. Zhang, J. You, D. Liu, H. O. Li, G. Cao, M. Xiao, and G. P. Guo, Sci Rep **5**(1), 16113 (2015).

[17] K. Lee, G. Kulkarni, and Z. Zhong, Nanoscale **8**(14), 7755–7760 (2016).

[18] N. Papadopoulos, P. Gehring, K. Watanabe, T. Taniguchi, H. S. J. van der Zant, and G. A. Steele, Phys. Rev. B **101**(16), 165303 (2020).

[19] T. R. Devidas, I. Keren, and H. Steinberg, Nano Lett. **21**(16), 6931–6937 (2021).

[20] R. Krishnan, S. Biswas, Y. L. Hsueh, H. Ma, R. Rahman, and B. Weber, Nano Lett. **23**(13), 6171–6177 (2023).

[21] S. Davari, J. Stacy, A. Mercado, J. Tull, R. Basnet, K. Pandey, K. Watanabe, T. Taniguchi, J. Hu, and H. Churchill, Phys. Rev. Appl. **13**(5), 054058 (2020).

[22] P. Kumar, H. Kim, S. Tripathy, K. Watanabe, T. Taniguchi, K. S. Novoselov, and D. Kotekar-Patil, Nanoscale **15**(45), 18203–18211 (2023).

[23] R. Tenne, L. Margulis, M. Genut, and G. Hodes, Nature **360**, 444 (1992).

[24] M. Remskar, Z. Skraba, F. Cléton, R. Sanjinés, and F. Lévy, Appl. Phys. Lett. **69**(3), 351–353 (1996).

[25] G. Seifert, T. Köhler, and R. Tenne, J. Phys. Chem. B **106**(10), 2497–2501 (2002).

[26] W. Schottky, Zeitschrift für Physik **113**(5), 367–414 (1939).

[27] C. Gong, L. Colombo, R. M. Wallace, and K. Cho, Nano Letters **14**(4), 1714–1720 (2014).

[28] K. Sotthewes, R. van Bremen, E. Dollekamp, T. Boulogne, K. Nowakowski, D. Kas, H. J. W. Zandvliet, and P. Bampoulis, The Journal of Physical Chemistry C **123**(9), 5411–5420 (2019).

[29] P. C. Shen, C. Su, Y. Lin, A. S. Chou, C. C. Cheng, J. H. Park, M. H. Chiu, A. Y. Lu, H. L. Tang, M. M. Tavakoli, G. Pitner, X. Ji, Z. Cai, N. Mao, J. Wang, V. Tung, J. Li, J. Bokor, A. Zettl, C. I. Wu, T. Palacios, L. J. Li, and J. Kong, Nature **593**(7858), 211–217 (2021).

[30] W. Li, X. Gong, Z. Yu, L. Ma, W. Sun, S. Gao, Ç. Köroğlu, W. Wang, L. Liu, T. Li, H. Ning, D. Fan, Y. Xu, X. Tu, T. Xu, L. Sun, W. Wang, J. Lu, Z. Ni, J. Li, X. Duan, P. Wang, Y. Nie, H. Qiu, Y. Shi, E. Pop, J. Wang, and X. Wang, Nature **613**(7943), 274–279 (2023).

[31] S. Das, H. Y. Chen, A. V. Penumatcha, and J. Appenzeller, Nano Letters **13**(1), 100–105 (2013).

[32] M. Serra, R. Arenal, and R. Tenne, Nanoscale **11**(17), 8073–8090 (2019).

[33] J. L. Musfeldt, Y. Iwasa, and R. Tenne, Physics Today **73**(8), 42–48 (2020).

[34] F. Qin, T. Ideue, W. Shi, X. X. Zhang, M. Yoshida, A. Zak, R. Tenne, T. Kikitsu, D. Inoue, D. Hashizume, and Y. Iwasa, Nano Letters **18**(11), 6789–6794 (2018).

[35] S. Fathipour, M. Remskar, A. Varlec, A. Ajoy, R. Yan, S. Vishwanath, S. Rouvimov, W. S. Hwang, H. G. Xing, D. Jena, and A. Seabaugh, Appl. Phys. Lett. **106**(2), 022114 (2015).

[36] S. Reinhardt, L. Pirker, C. Bäuml, M. Remškar, and A. K. Hüttel, physica status solidi (RRL) – Rapid Research Letters **13**(11), 1900251 (2019).

[37] R. J. Wu, S. Udyavara, R. Ma, Y. Wang, M. Chhowalla, T. Birol, S. J. Koester, M. Neurock, and K. A. Mkhoyan, Phys. Rev. Materials **3**(11), 111001 (2019).

[38] M. Remskar, A. K. Hüttel, T. V. Shubina, A. Seabaugh, S. Fathipour, R. Lawrowski, and R. Schreiner, Israel Journal of Chemistry **62**(3-4), e202100100 (2022).

[39] R. T. K. Schock, J. Neuwald, W. Möckel, M. Kronseder, L. Pirker, M. Remškar, and A. K. Hüttel, Advanced Materials **35**(13), 2209333 (2023).

[40] K. Otsuka, N. Fang, D. Yamashita, T. Taniguchi, K. Watanabe, and Y. K. Kato, Nat Commun **12**(1), 3138 (2021).

[41] A. Castellanos-Gomez, M. Buscema, R. Molenaar, V. Singh, L. Janssen, H. S. J. van der Zant, and G. A. Steele, 2D Mater. **1**(1), 011002 (2014).

[42] R. Nitsche, Journal of Physics and Chemistry of Solids **17**(1-2), 163–165 (1960).

[43] M. Remškar, Z. Škraba, M. Regula, C. Ballif, R. Sanjinés, and F. Lévy, Advanced Materials **10**(3), 246–249 (1998).

[44] D. R. Kazanov, A. V. Poshakinskiy, V. Y. Davydov, A. N. Smirnov, I. A. Eliseyev, D. A. Kirilenko, M. Remškar, S. Fathipour, A. Mintairov, A. Seabaugh, B. Gil, and T. V. Shubina, Applied Physics Letters **113**(10), 101106 (2018).

[45] P. Jarillo-Herrero, S. Sapmaz, C. Dekker, L. P. Kouwenhoven, and H. S. J. van der Zant, Nature **429**(6990), 389–392 (2004).

[46] J. Cao, Q. Wang, and H. Dai, Nature Materials **4**(10), 745–749 (2005).

[47] W. Dong, Z. Dai, L. Liu, and Z. Zhang, Advanced Materials **36**(22), 2303014 (2024).

[48] S. Engels, A. Epping, C. Volk, S. Korte, B. Voigtländer, K. Watanabe, T. Taniguchi, S. Trellenkamp, and C. Stampfer, Applied Physics Letters **103**(7), 073113 (2013).

[49] J. I. A. Li, C. Tan, S. Chen, Y. Zeng, T. Taniguchi, K. Watanabe, J. Hone, and C. R. Dean, Science **358**(6363), 648–652 (2017).

[50] L. Banszerus, B. Frohn, A. Epping, D. Neumaier, K. Watanabe, T. Taniguchi, and C. Stampfer, Nano Letters **18**(8), 4785–4790 (2018).

[51] M. Eich, R. Pisoni, H. Overweg, A. Kurzmann, Y. Lee, P. Rickhaus, T. Ihn, K. Ensslin, F. Herman, M. Sigrist, K. Watanabe, and T. Taniguchi, Phys. Rev. X **8**(3), 031023 (2018).

[52] H. Overweg, H. Eggimann, X. Chen, S. Slizovskiy, M. Eich, R. Pisoni, Y. Lee, P. Rickhaus, K. Watanabe, T. Taniguchi, V. Fal'ko, T. Ihn, and K. Ensslin, Nano Lett. **18**(1), 553–559 (2018).

[53] J. R. Lince, D. J. Carré, and P. D. Fleischauer, Physical Review B **36**(3), 1647–1656 (1987).

[54] W. Mönch, Applied Physics Letters **72**(15), 1899–1901 (1998).

[55] C. Kim, I. Moon, D. Lee, M. S. Choi, F. Ahmed, S. Nam, Y. Cho, H. J. Shin, S. Park, and W. J. Yoo, ACS Nano **11**(2), 1588–1596 (2017).

[56] A. Chanana and S. Mahapatra, Journal of Applied Physics **119**(1), 014303 (2016).

[57] J. R. Chen, P. M. Odenthal, A. G. Swartz, G. C. Floyd, H. Wen, K. Y. Luo, and R. K. Kawakami, Nano Lett. **13**(7), 3106–3110 (2013).

[58] A. Dankert, L. Langouche, M. V. Kamalakar, and S. P. Dash, ACS Nano **8**(1), 476–482 (2014).

[59] M. Farmanbar and G. Brocks, Advanced Electronic Materials **2**(4), 1500405 (2016).

[60] G. Pande, J. Y. Siao, W. L. Chen, C. J. Lee, R. Sankar, Y. M. Chang, C. D. Chen, W. H. Chang, F. C. Chou, and M. T. Lin, ACS Appl. Mater. Interfaces **12**(16), 18667–18673 (2020).

[61] H. Gao, J. Suh, M. C. Cao, A. Y. Joe, F. Mujid, K. H. Lee, S. Xie, P. Poddar, J. U. Lee, K. Kang, P. Kim, D. A. Muller, and J. Park, Nano Lett. **20**(6), 4095–4101 (2020).

[62] J. Jiang, L. Xu, C. Qiu, and L. M. Peng, Nature **616**(7957), 470–475 (2023).

[63] M. Liu, S. Shahi, S. Fathipour, W. Hwang, M. Remskar, A. Seabaugh, and H. Li, Improvement of Metal-Semiconductor Contact from Schottky to Ohmic by Cu Doping in Transition Metal Dichalcogenide Transistors, in: 2018 IEEE 13th Nanotechnology Materials and Devices Conference (NMDC), (IEEE, Portland, OR, USA, October 2018), pp. 1–4.

[64] S. G. Louie and M. L. Cohen, Physical Review B **13**(6), 2461–2469 (1976).

[65] S. Lee, X. Wang, H. Shin, N. Ali, T. D. Ngo, E. Hwang, G. H. Kim, G. Y. Yeom, K. Watanabe, T. Taniguchi, and W. J. Yoo, ACS Appl. Electron. Mater. (2024).

[66] I. A. Eliseyev, B. R. Borodin, D. R. Kazanov, A. V. Poshakinskiy, M. Remškar, S. I. Pavlov, L. V. Kotova, P. A. Alekseev, A. V. Platonov, V. Y. Davydov, and T. V. Shubina, Advanced Optical Materials **11**(15), 2202782 (2023).

[67] P. Bolshakov, C. M. Smyth, A. Khosravi, P. Zhao, P. K. Hurley, C. L. Hinkle, R. M. Wallace, and C. D. Young, ACS Applied Electronic Materials **1**(2), 210–219 (2019).

[68] R. Mahlouji, Y. Zhang, M. A. Verheijen, J. P. Hofmann, W. M. M. Kessels, A. A. Sagade, and A. A. Bol, ACS Applied Electronic Materials **3**(7), 3185–3199 (2021).

[69] B. J. Lee, B. J. Lee, J. Lee, J. W. Yang, and K. H. Kwon, Thin Solid Films **637**(September), 32–36 (2017).

[70] J. J. Schwartz, H. J. Chuang, M. R. Rosenberger, S. V. Sivaram, K. M. McCreary, B. T. Jonker, and A. Centrone, ACS Applied Materials & Interfaces **11**(28), 25578–25585 (2019).

[71] A. Jain, P. Bharadwaj, S. Heeg, M. Parzefall, T. Taniguchi, K. Watanabe, and L. Novotny, Nanotechnology **29**(26), 265203 (2018).

[72] J. Pető, T. Ollár, P. Vancsó, Z. I. Popov, G. Z. Magda, G. Dobrik, C. Hwang, P. B. Sorokin, and L. Tapasztó, Nature Chemistry **10**(12), 1246–1251 (2018), Number: 12 Publisher: Nature Publishing Group.

[73] S. Reinhardt, C. Butschkow, S. Geissler, A. Dirnaichner, F. Olbrich, C. Lane, D. Schröer, and A. K. Hüttel, Computer Physics Communications **234**, 216 (2019).

Graphical Table of Contents

GTOC image:
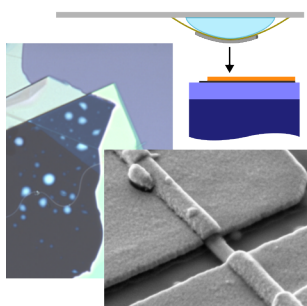
Clean and defect-free MoS_2 nanotubes are highly promising as novel material for quantum electronic devices. With this in mind, we look at device fabrication methods originally developed for planar, 2d transition metal dichalcogenides, and discuss their implementation for single MoS_2 nanotubes and -ribbons. This includes various transfer and assembly methods as well as the choice of contact materials.